Carbon 110 (2016) 278–285

Contents lists available at ScienceDirect

Carbon

journal homepage: www.elsevier.com/locate/carbon

Carbon dots as inhibitors of virus by activation of type I interferon response

Ting Du [a, 1], Jiangong Liang [a, 1], Nan Dong [b], Lin Liu [a], Liurong Fang [b], Shaobo Xiao [b, **, 2], Heyou Han [a, *, 2]

[a] State Key Laboratory of Agricultural Microbiology, College of Food Science and Technology, College of Science, Huazhong Agricultural University, Wuhan 430070, PR China
[b] State Key Laboratory of Agricultural Microbiology, College of Veterinary Medicine, Huazhong Agricultural University, Wuhan 430070, PR China

ARTICLE INFO

Article history:
Received 29 June 2016
Received in revised form
13 September 2016
Accepted 14 September 2016
Available online 15 September 2016

ABSTRACT

Carbon dots (CDs) has shown exciting potential in the field of bioscience and biotechnology due to their low toxicity, biological and ecological friendliness and desirable performance characteristics of quantum dots (QDs). However, the effects of CDs on viruses are still largely unknown. In this study, we investigate the effect of CDs on the replication of virus by using pseudorabies virus (PRV) and porcine reproductive and respiratory syndrome virus (PRRSV) as the models of DNA virus and RNA virus, respectively. Analyses of virus titers and the expression of viral proteins demonstrate that cells treated with CDs can significantly inhibit the multiplication of PRV and PRRSV. In mechanism, CDs treatment dramatically induces interferon-α (IFN-α) production and the expression of IFN-stimulating genes (ISGs) which in turn inhibits virus replication. Taken together, these results reveal a previously undefined role of CDs and provide a new strategy to develop antiviral agents.

1. Introduction

Carbon dots (CDs), a fascinating class of carbon nanomaterial family with a size below 10 nm, were discovered accidentally in 2004 [1]. Similar to semiconductor quantum dots (QDs), the fluorescence (FL) properties of CDs are attributed to passivated defects on the carbon particle surface [2]. CDs have attracted considerable attention in recent years as potential competitors of conventional semiconductor QDs due to their low toxicity, excellent biocompatibility, low cost and chemical inertness [3–7]. As a group of newly emerged fluorescent nanomaterials, CDs have presented enormous potential as versatile nanomaterials in a wide range of fields, such as bioimaging, sensing, drug delivery, photodynamic therapy, photocatalysis and energy conversion/storage devices [8–17]. Currently, nanoscale materials have sprung up as fresh antiviral agents because of their unique chemical and physical properties [18–22]. However, little information is available about the potential effects of CDs on virus.

Pseudorabies virus (PRV), a swine neurotropic herpesvirus that causes devastating disease and economic losses worldwide, contains a double stranded DNA genome and is a useful model for the study of herpesvirus biology [23,24]. Porcine reproductive and respiratory syndrome virus (PRRSV), an enveloped single-stranded positive-sense RNA virus, belongs to the family *Arteriviridae*, genus *Arterivirus* [25,26]. Since its emergence in the late 1980s, PRRSV has been a threat to the swine industry worldwide, causing enormous economic losses due to severe reproductive failure in sows and respiratory distress in piglets and growing pigs [27,28]. Unfortunately, the control of PRRSV and PRV is mainly performed by using traditional strategies or vaccines currently, indicating the necessity of developing novel antiviral drugs.

In the present study, we evaluated the antiviral effects of CDs and demonstrated that cells treated with CDs suppress the replication of PRV and PRRSV probably by activating antiviral type I interferon response.

* Corresponding author.
** Corresponding author.
E-mail addresses: vet@mail.hzau.edu.cn (S. Xiao), hyhan@mail.hzau.edu.cn (H. Han).
[1] These authors contributed equally.
[2] These authors jointly supervised this work.

http://dx.doi.org/10.1016/j.carbon.2016.09.032
0008-6223/

2. Experimental section

2.1. Synthesis of CDs

The CDs were prepared as previously reported with slight modifications [29]. Briefly, 0.20 g of PEG-diamine and 0.40 g of ascorbic acid were mixed and then ground into a uniform powder in an agate mortar. Then the mixture was transferred to a Teflon-lined autoclave chamber (50 mL) and heated at 180 °C for 1 h. After the reaction, the obtained dark brown mixture was dissolved in 10 mL of ultrapure water (Milli-Q, Millipore, 18.2 MΩ resistivity). The supernatant was centrifuged at 12000 rpm for 10 min to remove the large dots. Next, the solution was dialyzed against ultrapure water (Mill-Q, Millipore, 18.2 MΩ resistivity) using a dialysis membrane for 24 h to remove the unreacted low molecular weight by-products. The as-prepared CDs were stored at 4 °C for further use.

2.2. Cells and viruses

Monkey kidney (MARC-145) cells were purchased from the American Type Culture Collection (ATCC no. CRL-1223). Porcine kidney (PK-15) cells were purchased from the China Center for Type Culture Collection (CCTCC, Wuhan, China). Both types of cells were maintained in Dulbecco's modified Eagle's medium (DMEM, Invitrogen) supplemented with 10% fetal bovine serum (FBS) in a humidified incubator at 37 °C under 5% CO_2. PRRSV strain WUH3, which was isolated in China at the end of 2006, was propagated in MARC-145 cells [30]. PRV strain Ea, a wild virulent strain isolated in China [31], was propagated in PK-15 cells.

2.3. Cytotoxicity assay

The cytotoxicity of the CDs was determined as previously described [32]. Briefly, PK-15 cells and MARC-145 cells at a confluence of 90% in 96-well plates, were treated with 0.250 mg/mL, 0.125 mg/mL CDs and control DMEM (2% FBS) in triplicate, in a total of 100 μL growth medium separately for 12, 24, 36 and 48 h, followed by the addition of 20 μL MTT solution (3-[4,5-dimethylthiazol-2-thiazolyl]-2,5-diphenyl tetrazolium bromide, Sigma) to each well, and then incubation at 37 °C for 4 h. After that, the supernatant was removed, and the formazan crystals were dissolved in 150 μL/well dimethylsulfoxide. The absorption values were measured at 570 nm by using an Enzyme Linked Immunosorbent Assay (ELISA) microplate reader and the cell viability percentage was calculated.

2.4. Viral replication analysis

PK-15 cells in a monolayer were incubated with control DMEM (2% FBS) and CDs at 37 °C for 2 h, followed by infection with PRV at a multiplicity of infection (MOI) of 1.0 for 1 h. Next, the infected cells were washed twice with PBS, then supplemented with DMEM (2% FBS) and CDs for further incubation. Medium supernatant and cell lysate containing progeny PRV were collected separately at 12, 18 and 24 hpi (hour post infection). All samples were stored at −80 °C, and after three rounds of freeze-thaw, the cell debris was removed by centrifugation at 3000 rpm for 15 min. The infectivity of virions collected at different infection time points was determined by plaque assays.

MARC-145 cells in a monolayer were incubated with control DMEM (2% FBS) and CDs at 37 °C for 2 h, followed by infection with PRRSV at an MOI of 1.0 for 1 h. Next, the infected cells were washed twice with PBS, and then supplemented with DMEM (2% FBS) and CDs for further incubation. Medium supernatant and cell lysate containing progeny PRRSV were collected separately at 24, 36 and 48 hpi. The following steps are consistent with those for PK-15 cells.

2.5. Viral plaque assays

Plaque assays for PRV were performed as described previously with slight modifications [33]. Briefly, 95% confluent PK-15 cells cultured in 6-well tissue culture plates were infected for 1 h with 10-fold serial dilutions (1.0 mL) containing PRV. After washing with phosphate-buffered saline (PBS, pH 7.4), cells were overlaid with 1.8% (w/v) low melting point agarose (Promega) containing 2× DMEM supplemented with 3% FBS. Plaques were counted 3–4 dpi (days post infection) after staining with neutral red mixed with PBS at a 1:1 ratio for 2 h at 37 °C. The average plaque number and standard deviations were calculated from three independent experiments and the virus titers were presented as plaque forming units (PFU/mL).

Plaque assays for PRRSV were performed as previously described [34]. 95% confluent MARC-145 cells cultured in 6-well tissue culture plates were infected for 1 h with 10-fold serial dilutions (1.0 mL) containing PRRSV. The following steps are in accordance with those for PRV.

2.6. $TCID_{50}$ assay

PK-15 cells were seeded into 96-well plates in DMEM (10% FBS) until the cells reached 90–100% confluence. 100 μL samples of 10-fold dilutions containing PRV and paired control DMEM (2% FBS) were inoculated in eight replicates per dilution. After absorption for 1 h, $TCID_{50}$ cultures were discarded and supplemented with DMEM containing 2% FBS. Then, the infected cells were cultured in an incubator at 37 °C/5% CO_2 for 2–4 days.

Subsequently, 100 μL samples of 10-fold dilutions containing PRRSV and paired control DMEM (2% FBS) were added into 96-well plates in eight replicates per dilution, followed by seeding MARC-145 cells into each 96-well plate and incubation at 37 °C/5% CO_2. Viral CPE was monitored for 3–5 days. The PRRSV and PRV titers were calculated by using the Reed-Muench method [35] and presented as $TCID_{50}$ per microliter.

2.7. Western blot

PK-15 cells in 6-well plates infected with PRV in the presence or absence of CDs were harvested at 24 hpi and MARC-145 cells in 6-well plates infected with PRRSV in the presence or absence of CDs were collected at 48 hpi, followed by rinsing three times with PBS and then treatment with 150 μL/well lysis buffer (LBA) (4% sodium dodecyl sulfate, 3% DL-dithiothreitol, 65 mM Tris–HCl (pH 6.8, 40% glycerin)). Equivalent amounts of cell lysates were denatured in 5× Sodium dodecyl sulfate (SDS) loading buffer by boiling at 95 °C for 10 min and were then electrophoresed on 12% sodium dodecyl sulfate polyacrylamide gel electrophoresis (SDS-PAGE). Subsequently, the separated proteins were transferred to 0.2 μm PVDF Membrane (Millipore). The membranes were blocked with 10% (w/v) nonfat dry milk for 4 h at room temperature and incubated with primary antibodies overnight at 4 °C, followed by exposure to HRP-conjugated secondary antibodies for 2 h at 37 °C. β-actin was detected as loading control. Protein bands were visualized using the Clarity Enhanced Chemiluminescence (ECL) reagent (Bio-Rad, Hercules, CA) [36].

2.8. Indirect immunofluorescence assays

Approximately 70–80% confluent PK-15 cells were mock-treated or treated with CDs at 37 °C for 2 h and then infected

with PRV at 0.5 MOI for 1 h. After infection, PK-15 cells were cultured with control DMEM (2% FBS) or CDs and fixed with cold 4% paraformaldehyde at 24 hpi. After permeabilization with methanol (−20 °C), the PRV-infected cells were detected with rabbit polyclonal antibody directed against the PRV gD (1:100) protein and FITC-labeled goat anti-rabbit IgG antibody (1:500). The cell nucleus was stained with 4′,6-diamidino-2-phenylindole (DAPI, Invitrogen) [37]. Fluorescence images were acquired using an Olympus IX73 confocal laser scanning microscope.

Approximately 70–80% confluent MARC-145 cells were mock-treated or treated with CDs at 37 °C for 2 h and then infected with PRRSV at 0.5 MOI for 1 h. After infection, MARC-145 cells were cultured with control DMEM (2% FBS) or CDs and fixed with cold 4% paraformaldehyde at 48 hpi. After permeabilization with methanol (−20 °C), the PRRSV-infected cells were detected with mouse monoclonal antibody directed against the PRRSV N protein (1:100) and FITC-labeled goat anti-mouse IgG antibody (1:500). Then the following steps are consistent with those for PK-15 cells.

2.9. RNA exaction and quantitative real-time RT-PCR

MARC-145 cells grown in 24-well plates were mock-treated or treated with CDs at 37 °C for 2 h and then cells were mock-transfected or transfected with 1.0 μg of poly(I:C). Total RNA was extracted using TRIzol reagent (Invitrogen) at 24 h. 1.0 μg of each sample were reverse transcribed into cDNA using a Transcriptor First Strand cDNA Synthesis Kit (Roche), then 1 μL of the resulting cDNA was used in a SYBR green PCR assay (Applied Biosystems, U.S.A.). The individual mRNA transcript in each sample was assayed three times. The PCR procedure was as follows: pre-denaturation at 95 °C for 10 min, then 40 cycles of 15 s at 95 °C, 15 s at 58 °C and 40 s at 72 °C. The primers (Table S1) were designed by Primer Express software (version 3.0, Applied Biosystems, Carlsbad, CA).

2.10. Statistical analysis

An independent *t*-test or one-way ANOVA test was applied to analyze the experimental data. Data are shown as the mean ± SE. Statistical significance was determined with a p value < 0.05 and p value < 0.01.

3. Results and discussion

3.1. Characterization of CDs

The morphology and the optical properties of the as-prepared CDs are presented in Fig. 1. As displayed in Fig. 1(A), at an excitation wavelength of 350 nm, a maximum fluorescence emission peak at 435 nm was obtained in the Photoluminescence (PL) emission spectrum of CDs, indicating a blue light emission. When the excitation wavelength was increased from 340 to 400 nm, there was a maximal emission wavelength shift of ~40 nm, which is consistent with a previous study [38]. The excitation-dependent FL behavior of CDs is due to the co-existence of different sizes and a distribution of different surface states in each sample (Fig. 1(B)). Fig. 1(C) shows the TEM image of the as-prepared CDs, from which we can see that these small CDs were monodispersed and mostly composed of uniform spherical shapes. The top right corner of Fig. 1(C) presents the high-resolution TEM (HRTEM) images of CDs with an average size of 4.5 ± 0.9 nm, and the hydrodynamic size distribution measured by dynamic light scattering (DLS) was in the 3–7 nm range with an average size of 4.7 nm (Fig. 1(D)). The zeta-potential of CDs was −15.7 ± 1.65 mV.

The surface functional groups of the obtained CDs were analyzed using the Fourier transform infrared (FTIR) spectroscopy. As shown in Fig. S1, the characteristic absorption bands at 3000–3500 cm^{-1} were attributable to the stretching vibrations of

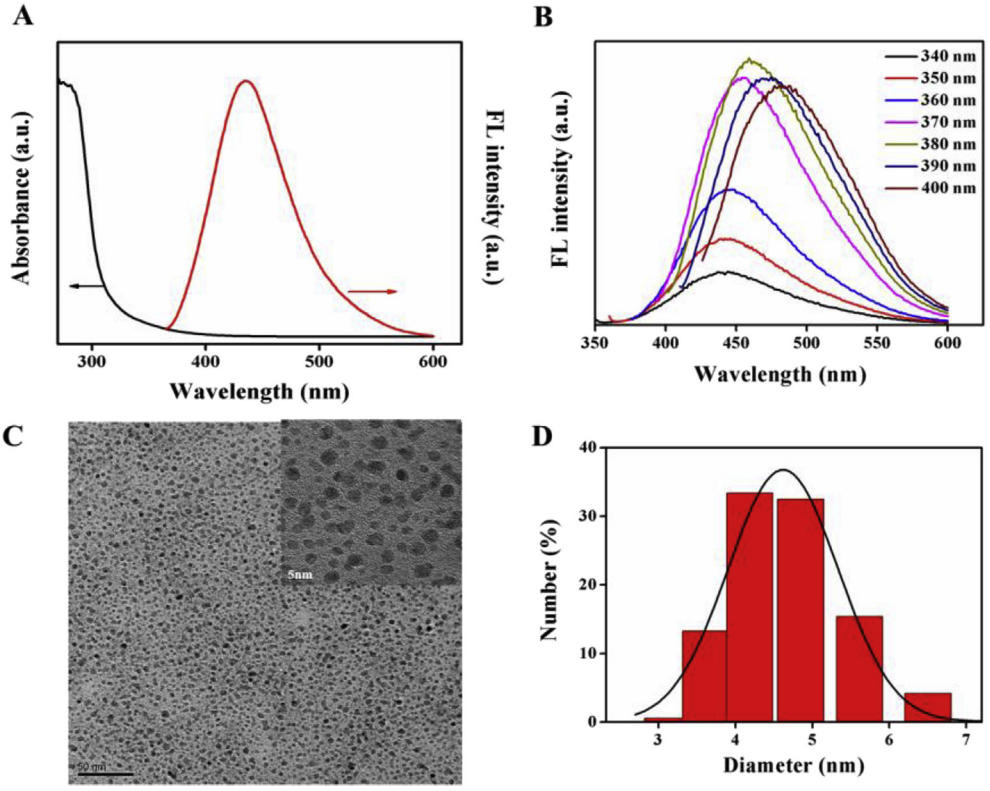

Fig. 1. (A) UV–vis absorption and fluorescence spectra of CDs. (B) Fluorescent emission spectra of CDs at different excitation wavelengths (from 340 to 400 nm). (C) TEM and HRTEM of as-prepared CDs. (D) The particle size distribution of CDs. (A colour version of this figure can be viewed online.)

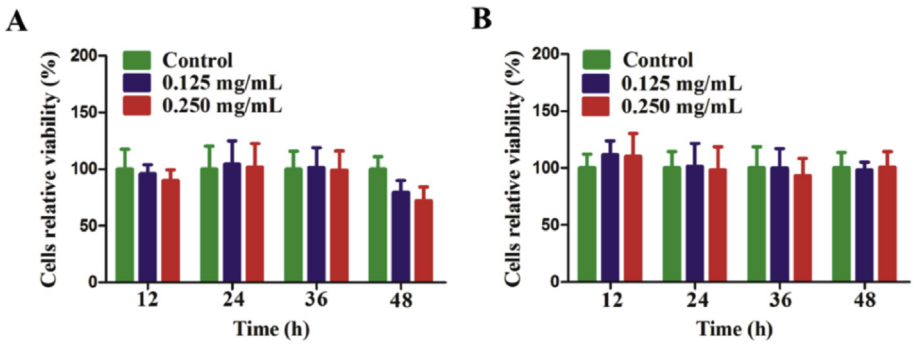

Fig. 2. Cytotoxicity of different concentrations of CDs by MTT assay. PK-15 cells (A) and MARC-145 cells (B) were incubated with CDs separately for 12, 24, 36 and 48 h. Error bars represent the standard deviation from three repeated experiments. (A colour version of this figure can be viewed online.)

O–H and N–H [9,39]. The high-intensity peaks around 2875 and 785 cm^{-1} corresponded to the stretching vibrations of the C–H. The band at 1730 cm^{-1} was assigned to the vibration of C=O, and the peaks around 1100, 1460, and 1630 cm^{-1} were related to vibrations of C–OH, C–NH and N–H bonds, respectively [40,41]. The results suggested that abundant hydrophilic groups were present on the surface of CDs.

Moreover, the chemical structure of CD was also investigated using X-ray photoelectron spectroscopy (XPS). In the overall XPS spectra (Fig. S2(A)), three evident peaks at 284.3, 399.5, and 531.5 eV could be attributed to C 1s, N 1s, and O 1s, respectively. The C 1s peak at 288.7, 285.7 and 284.3 eV might indicate that carbon is mostly in the form of C=O, C–N and C–C (Fig. S2(B)) [4]. The XPS spectrum of N 1s (Fig. S2(C)) confirmed the presence of N–H (400.9 eV) and N–$(C)_3$ (399.5 eV) bonds. The O 1s peak at 532.2 and 531.5 eV was associated with C–OH/C–O–C and C=O groups, respectively (Fig. S2(D)) [29,42]. The surface components of CDs determined by the XPS were in good agreement with the results of FTIR.

3.2. Toxicity of CDs on cells

To determine the effect of CDs treatment on the viability of PK-15 and MARC-145 cells, an MTT cytotoxicity assay was performed. As shown in Fig. 2, the viability of PK-15 and MARC-145 cells was more than 90% at 0.125 mg/mL of CDs after incubation separately for 12, 24, 36 and 48 h. Additionally, at a high concentration of 0.250 mg/mL CDs exhibited little toxicity to the cells and the viability of PK-15 cells was close to 72% after 48 h incubation (Fig. 2). Sun and co-workers reported that 50 μg/mL CDs are nontoxic to the selected cell lines [43]. Ray et al. also showed that, at a CDs exposure concentration of less than 0.5 mg/mL, the survival rate of cells ranged between 90 and 100% [44]. Our results for both PK-15 and MARC-145 cell lines were similar to the previous reports [43,44]. Thus, the concentration of 0.125 mg/mL CDs was used in the subsequent experiments.

3.3. CDs exhibit antiviral activity on PRV

To investigate the effect of CDs on PRV, viral replication was measured by plaque assay at a fixed CD concentration of 0.125 mg/mL. As depicted in Fig. 3(A) and (B), the virus titers of both intracellular and the supernatant were remarkably reduced in the presence of CDs compared with the control groups, indicating the potential antiviral activity of CDs against PRV.

PRV gD is a type I membrane glycoprotein, responsible for establishing stable binding of virions with host cell receptors and the subsequent fusion of the viral envelope with plasma membrane [23,45]. PRV VP16 is a tegument protein and a component of primary enveloped virions [46]. VP16 is highly conserved among Alphaherpesvirinae, playing multiple roles during induction of viral gene expression and viral egress [23]. To further confirm the antiviral efficiency of CDs on PRV, the indirect immunofluorescence assays and western blot analysis were performed to examine whether CDs inhibit the expression of PRV-gD and PRV-VP16 proteins. To this end, the pretreated cells or unpretreated cells were infected with PRV for 1 h, followed by incubation in the absence or presence of CDs. After 24 hpi, the cells were fixed and immunostained with specific antibody against PRV gD protein. As shown in Fig. 4(A), the green fluorescence signal of the group treated with CDs was dramatically decreased compared with the control. Consistent with the results of indirect immunofluorescence assays

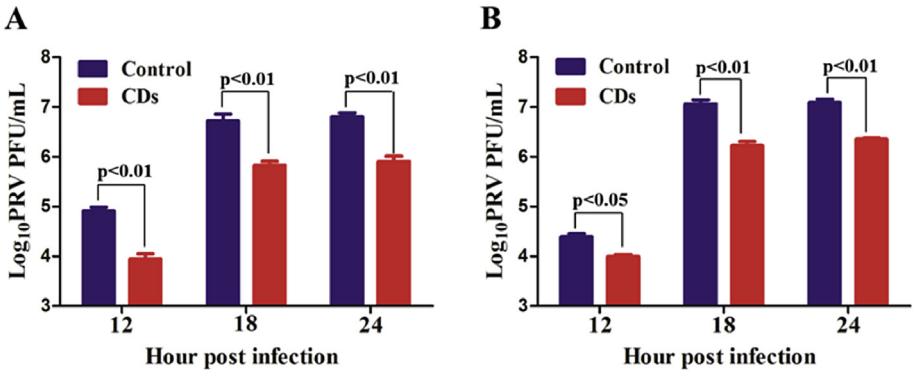

Fig. 3. Replication process of PRV (A and B) in the absence and presence of 0.125 mg/mL CDs. The virus titer of intracellular (A) and the virus titer of supernatant (B). Error bars represent the standard deviation from three repeated experiments. (A colour version of this figure can be viewed online.)

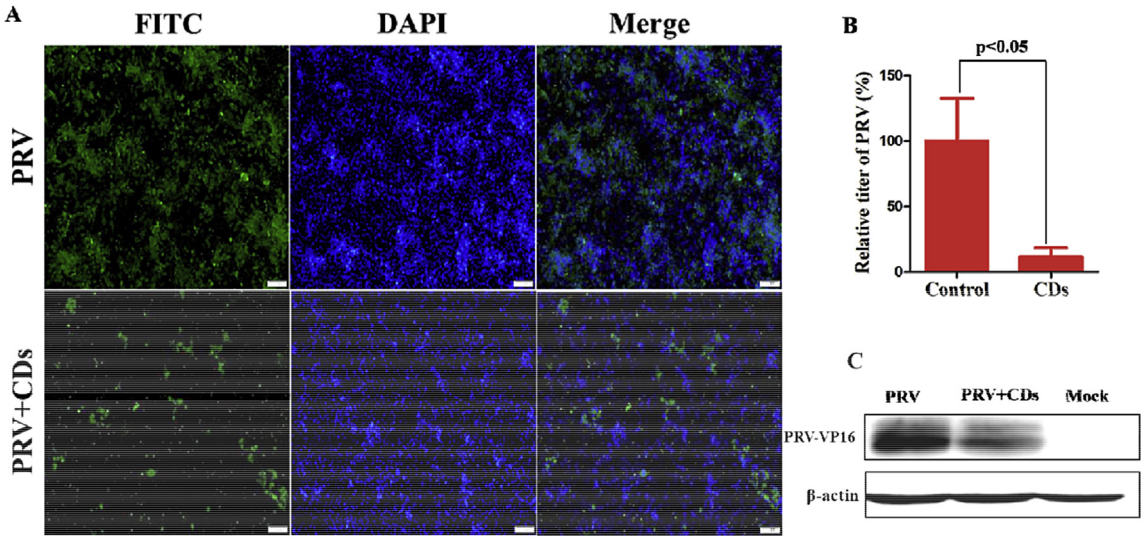

Fig. 4. The effect of CDs on PRV. (A) Indirect immunofluorescence assays of PRV-infected PK-15 cells in the absence and presence of 0.125 mg/mL CDs. The excitation wavelength of DAPI and FITC were 340–390 nm and 460–495 nm, respectively. Scale bars: 100 μm. (B) The relative titer of PRV in the absence and presence of 0.125 mg/mL CDs. Error bars represent the standard deviation from three repeated experiments. (C) Western blot analysis of the expression level of PRV-VP16 protein when 0.125 mg/mL CDs was added to PRV-infected cells at 24 hpi. β-actin was used as a loading control. (A colour version of this figure can be viewed online.)

(Fig. 4(A)), a marked reduction of viral relative titers (obtained by TCID50) was observed in the presence of CDs compared with the control (Fig. 4(B)). In addition, we detected an obviously down-regulated expression level of the PRV-VP16 protein by the western blot assay (Fig. 4(C)). Overall, these results ruled out the possibility that the aforementioned observed plaque reductions were caused by cellular toxicity of the CDs. In addition, we have carried out the experiment to test whether the fluorescence of CDs will influence the images of FITC and DAPI. As shown in Fig. S3, the fluorescence of CDs can be ignored in comparison with that of FITC and DAPI in Fig. 4(A). To further investigate if CDs can be taken by PK-15 cell, the fluorescence image were observed by using a confocal laser-scanning microscope (Nikon C1-si TE2000, Japan). Microscope images showed weak intracellular fluorescence, indicating that CDs can be taken by PK-15 cell (Fig. S4).

3.4. CDs exhibit antiviral activity on PRRSV

To investigate the antiviral spectrum of CDs, another RNA virus, PRRSV (classified within the family *Arteriviridae*) was used. During the viral infection cycle, the number of progeny infectious PRRSV in the presence of CDs was decreased markedly compared with the control group (Fig. 5), demonstrating the inhibitory properties of CDs against RNA virus.

PRRSV N, a sole structural component of viral capsid with a molecular weight of 15-kDa, performs the multiple functions of nuclear localization and N–N homodimerization during virus infection [47,48]. The inhibitory effects of CDs on the expression of PRRSV-N proteins were also analyzed by indirect immunofluorescence assays and Western blot analysis. As shown in Fig. 6(A), when compared with the untreated controls, the green fluorescence signal was apparently decreased, which directly reflected the reduction of PRRSV N protein expression level. This conclusion was corroborated by the results from western blot assay (Fig. 6(C)). Additionally, the relative titer of PRRSV decreased 88% after CDs treatment versus the untreated control (Fig. 6(B)). Collectively, these results further supported the conclusion that CDs could effectively inhibit the replication of PRRSV.

3.5. CDs activate type I interferon responses

Innate immune system is the first line of defense against invading pathogens and microorganisms [49]. Type I interferons (IFNs), including IFN-α and IFN-β, are the best known antiviral innate immune molecules with a powerful antiviral response to viral infection in the body [50]. As is well-known, the secreted IFN-

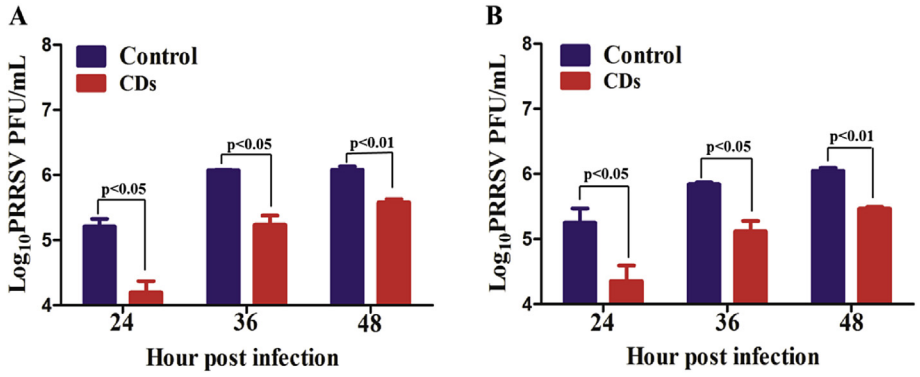

Fig. 5. Replication process of PRRSV (A and B) in the absence and presence of 0.125 mg/mL CDs. The virus titer of intracellular (A) and the virus titer of supernatant (B). Error bars represent the standard deviation from three repeated experiments. (A colour version of this figure can be viewed online.)

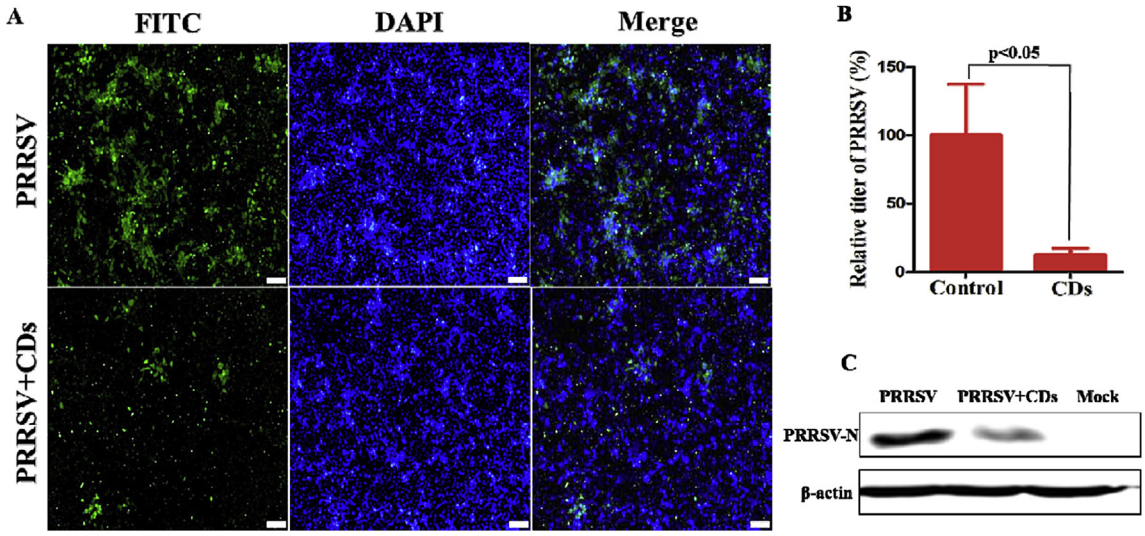

Fig. 6. The effect of CDs on PRRSV. (A) Indirect immunofluorescence assays of PRRSV-infected MARC-145 cells in the absence and presence of 0.125 mg/mL CDs The excitation wavelength of DAPI and FITC were 340–390 nm and 460–495 nm, respectively. Scale bars: 100 μm. (B) The relative titer of PRRSV in the absence and presence of 0.125 mg/mL CDs. Error bars represent the standard deviation from three repeated experiments. (C) Western blot analysis of the expression level of PRRSV-N protein when 0.125 mg/mL CDs was added to PRRSV-infected cells at 48 hpi. β-actin was used as a loading control. (A colour version of this figure can be viewed online.)

α/β initiate an intracellular signaling cascade, resulting in the activation of the expression of hundreds of IFN-stimulated genes (ISGs), which collectively suppress the replication of viruses [51,52]. To explore the possible mechanism(s) underlying the inhibitory effects of CDs, we focused on the effects of CDs on the expressions of IFN-α and the downstream ISGs. To this end, MARC-145 cells were mock-treated or treated with CDs for 24 h. Cells transfected with Poly(I:C) were used as positive controls. As shown in Fig. 7(A), the mRNA expression level of IFN-α in cells treated with CDs was 5.0-fold higher than that of the untreated control. As expected, a distinctly up-regulated expression of interferon inducible protein 10 (IP-10) (Fig. 7(B)), interferon stimulated gene 15 (ISG-15) (Fig. 7(C)) and interferon stimulated gene 54 (ISG-54) (Fig. 7(D)) could be observed in cells after CDs treatment, and the mRNA expressions of IP-10, ISG-15 and ISG-54 were 24.8-, 11.8- and 4.6-fold higher than those of the untreated controls. Together, these data suggested that the inhibitory effect of CDs was probably due to the activation of IFN-α and the production of ISGs. However, it cannot

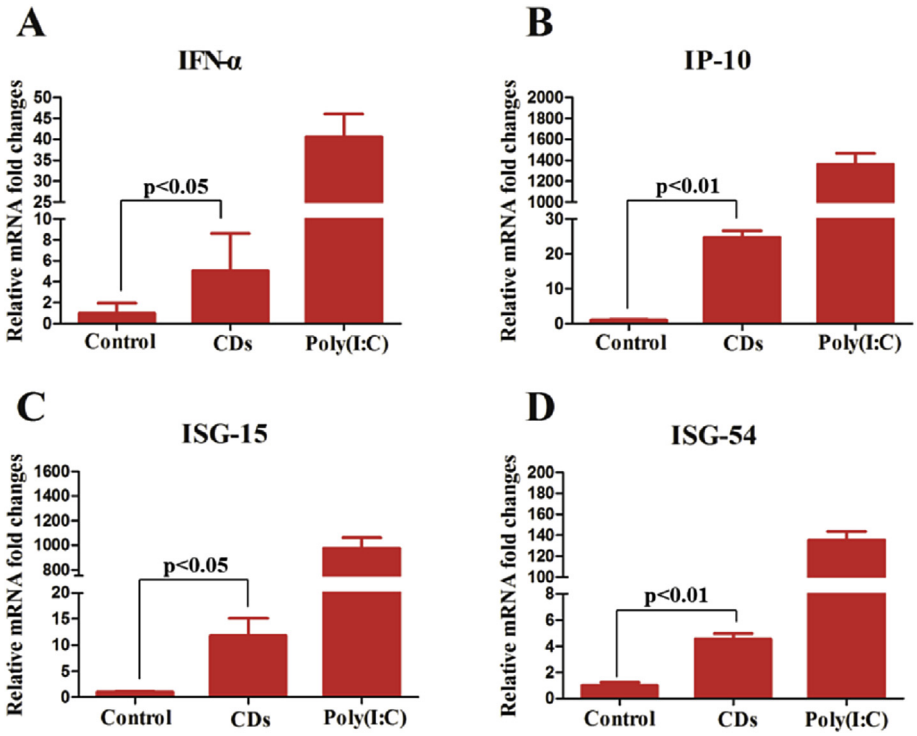

Fig. 7. Expression of cytokines in MARC-145 cells stimulated by 0.125 mg/mL CDs. The expressions of IFN-α (A), IP-10 (B), ISG-15 (C) and ISG-54 (D) were analyzed by Real-time RT-PCR using MARC-145 cDNA samples. Gene expression was normalized to that of GAPDH. Results are presented as the mean ± SD from three independent experiments in triplicate. (A colour version of this figure can be viewed online.)

rule out the possibility that there are other mechanism(s) utilized by CDs for their antiviral activity.

During the past decade, functional gold nanoparticles [20], silver nanoparticles [53], cuprous oxide nanoparticles [54], carbon-based nanomaterials [21], and silicon nanoparticles [55] have been reported to exhibit antiviral activity. However, the main antiviral effects of these nanomaterials are attributed to the direct inactivation of virus in vitro or the inhibition of viral entry into cells [56]. Meanwhile, our previous work investigated the interactions of CdTe QDs with PRV, and found that CdTe QDs can inhibit PRV replication by changing the structure of viral surface proteins, leading to the release of Cd^{2+} [57]. Thus, all of the aforementioned nanomaterials cannot suppress viral infection in the intracellular stage. In this study, we demonstrated for the first time that CDs have a strong inhibitory effect on the replication of PRV and PRRSV by inducing type I IFN production. It is well known that CDs can be prepared by different precursors, such as ascorbic acid [58], saccharides [59], watermelon peels [60], orange juice [61], chicken eggs [62], and so on, suggesting the possibility to synthesize more efficient antiviral reagents by using other CDs or conjugating CDs and functional molecules [63]. More importantly, carbon is an essential element in the human body and plays a crucial role in all living organisms [64], which has been verified to be nontoxic from cytotoxicity and in vivo toxicity evaluation [65–68]. Thus, the CDs-based drugs might have potential to be developed as a promising virucide in vivo.

Besides virus, such particles might also affect bacteria and even "good ones" needed in the organism. This is a very interesting issue and requires further study. It should be noted that the action mechanisms vary in inhibiting viral and bacterial replication. For example, interferons, which can be induced by CDs in our experiments, are efficient antiviral agents, but have a slight effect on bacteria.

4. Conclusion

In this study, we successfully synthesized CDs through solid-phase thermal reaction, and characterized CDs by standard spectroscopic techniques (Uv–vis, fluorescence and FTIR spectroscopy) as well as by DLS, XPS and TEM. The characterization results indicate that the CDs were well monodispersed on the surfaces with a uniform size and rich hydrophilic groups.

This is the first report showing that CDs have remarkable antiviral activity against DNA virus (PRV) and RNA virus (PRRSV) infection at a noncytotoxic concentration. The CDs can significantly inhibit the replication of PRV and PRRSV, which was confirmed by the analysis results of viral titers and viral protein expression. Mechanism study showed that CDs treatment activates the interferon-α production and the expression of interferon stimulated genes, which in turn inhibits viral replication. Additionally, the mRNA expressions of IFN-α, IP-10, ISG-15 and ISG-54 were 5.0–24.8-, 11.8- and 4.6-fold higher than those of the untreated controls. These encouraging results provide experimental basis for further research on CDs as a novel antiviral agent, and they also have important implications for understanding the antiviral relationship between CDs and many other viruses.

Acknowledgements

This research was supported by the National Natural Science Foundation of China (31225027, 21375043, 31490602, 31372439). The Key Technology R&D Programme of China (2015BAD12B02), and the Natural Science Foundation of Hubei Province (2014CFA009). We are also thankful to Prof. Hanchang Zhu for editing of the language. The authors declare no competing financial interest.

Appendix A. Supplementary data

Supplementary data related to this article can be found at http://dx.doi.org/10.1016/j.carbon.2016.09.032.

References

[1] X. Xu, R. Ray, Y. Gu, H.J. Ploehn, L. Gearheart, K. Raker, et al., Electrophoretic analysis and purification of fluorescent single-walled carbon nanotube fragments, J. Am. Chem. Soc. 126 (40) (2004) 12736–12737.
[2] L. Cao, X. Wang, M.J. Meziani, F. Lu, H. Wang, P.G. Luo, et al., Carbon dots for multiphoton bioimaging, J. Am. Chem. Soc. 129 (37) (2007) 11318–11319.
[3] S.Y. Lim, W. Shen, Z. Gao, Carbon quantum dots and their applications, Chem. Soc. Rev. 44 (1) (2015) 362–381.
[4] C. Shen, Y. Sun, J. Wang, Y. Lu, Facile route to highly photoluminescent carbon nanodots for ion detection, pH sensors and bioimaging, Nanoscale 6 (15) (2014) 9139–9147.
[5] H. Li, Z. Kang, Y. Liu, S.T. Lee, Carbon nanodots: synthesis, properties and applications, J. Mater. Chem. 22 (46) (2012) 24230–24253.
[6] A. Nagy, A. Steinbrück, J. Gao, N. Doggett, J.A. Hollingsworth, R. Iyer, Comprehensive analysis of the effects of CdSe quantum dot size, surface charge, and functionalization on primary human lung cells, ACS Nano 6 (6) (2012) 4748–4762.
[7] X. Li, M. Rui, J. Song, Z. Shen, H. Zeng, Carbon and graphene quantum dots for optoelectronic and energy devices: a review, Adv. Funct. Mater. 25 (31) (2015) 4929–4947.
[8] K. Jiang, S. Sun, L. Zhang, Y. Lu, A. Wu, C. Cai, et al., Red, green, and blue luminescence by carbon dots: full-color emission tuning and multicolor cellular imaging, Angew. Chem. Int. Ed. 54 (18) (2015) 5360–5363.
[9] Y. Guo, Z. Wang, H. Shao, X. Jiang, Hydrothermal synthesis of highly fluorescent carbon nanoparticles from sodium citrate and their use for the detection of mercury ions, Carbon 52 (2013) 583–589.
[10] C. Zhu, J. Zhai, S. Dong, Bifunctional fluorescent carbon nanodots: green synthesis via soy milk and application as metal-free electrocatalysts for oxygen reduction, Chem. Commun. 48 (75) (2012) 9367–9369.
[11] M. Zheng, S. Ruan, S. Liu, T. Sun, D. Qu, H. Zhao, et al., Self-targeting fluorescent carbon dots for diagnosis of brain cancer cells, ACS Nano 9 (11) (2015) 11455–11461.
[12] T. Feng, X. Ai, G. An, P. Yang, Y. Zhao, Charge-convertible carbon dots for imaging-guided drug delivery with enhanced in vivo cancer therapeutic efficiency, ACS Nano 10 (4) (2016) 4410–4420.
[13] Z. Song, F. Quan, Y. Xu, M. Liu, L. Cui, J. Liu, Multifunctional N, S co-doped carbon quantum dots with pH- and thermo-dependent switchable fluorescent properties and highly selective detection of glutathione, Carbon 104 (2016) 169–178.
[14] G.E. LeCroy, S.K. Sonkar, F. Yang, L.M. Veca, P. Wang, K.N. Tackett, et al., Toward structurally defined carbon dots as ultracompact fluorescent probes, ACS Nano 8 (5) (2014) 4522–4529.
[15] H. Wang, J. Di, Y. Sun, J. Fu, Z. Wei, H. Matsui, et al., Biocompatible PEG-chitosan@carbon dots hybrid nanogels for two-photon fluorescence imaging, near-infrared light/pH dual-responsive drug carrier, and synergistic therapy, Adv. Funct. Mater. 25 (34) (2015) 5537–5547.
[16] J. Wang, Z. Zhang, S. Zha, Y. Zhu, P. Wu, B. Ehrenberg, et al., Carbon nanodots featuring efficient FRET for two-photon photodynamic cancer therapy with a low fs laser power density, Biomaterials 35 (34) (2014) 9372–9381.
[17] L. Zhou, Y. Lin, Z. Huang, J. Ren, X. Qu, Carbon nanodots as fluorescence probes for rapid, sensitive, and label-free detection of Hg^{2+} and biothiols in complex matrices, Chem. Commun. 48 (8) (2012) 1147–1149.
[18] I. Papp, C. Sieben, K. Ludwig, M. Roskamp, C. Böttcher, S. Schlecht, et al., Inhibition of influenza virus infection by multivalent sialic-acid functionalized gold nanoparticles, Small 6 (24) (2010) 2900–2906.
[19] J.C. Trefry, D.P. Wooley, Silver nanoparticles inhibit vaccinia virus infection by preventing viral entry through a macropinocytosis-dependent mechanism, J. Biomed. Nanotechnol. 9 (9) (2013) 1624–1635.
[20] D. Baram-Pinto, S. Shukla, A. Gedanken, R. Sarid, Inhibition of HSV-1 attachment, entry, and cell-to-cell spread by functionalized multivalent gold nanoparticles, Small 6 (9) (2010) 1044–1050.
[21] A. Muñoz, D. Sigwalt, B.M. Illescas, J. Luczkowiak, L. Rodríguez-Pérez, I. Nierengarten, et al., Synthesis of giant globular multivalent glycofullerenes as potent inhibitors in a model of Ebola virus infection, Nat. Chem. 8 (1) (2016) 50–57.
[22] S. Ye, K. Shao, Z. Li, N. Guo, Y. Zuo, Q. Li, et al., Antiviral activity of graphene oxide: how sharp edged structure and charge matter, ACS Appl. Mater. Interfaces 7 (38) (2015) 21571–21579.
[23] L.E. Pomeranz, A.E. Reynolds, C.J. Hengartner, Molecular biology of pseudorabies virus: impact on neurovirology and veterinary medicine, Microbiol. Mol. Biol. Rev. 69 (3) (2005) 462–500.
[24] X. Sui, J. Yin, X. Ren, Antiviral effect of diammonium glycyrrhizinate and lithium chloride on cell infection by pseudorabies herpesvirus, Antivir. Res. 85 (2) (2010) 346–353.

[25] C.J. Nelsen, M.P. Murtaugh, K.S. Faaberg, Porcine reproductive and respiratory syndrome virus comparison: divergent evolution on two continents, J. Virol. 73 (1) (1999) 270–280.
[26] E.J. Snijder, M. Kikkert, Y. Fang, Arterivirus molecular biology and pathogenesis, J. Gen. Virol. 94 (10) (2013) 2141–2163.
[27] M.P. Murtaugh, T. Stadejek, J.E. Abrahante, T.T. Lam, F.C.C. Leung, The ever-expanding diversity of porcine reproductive and respiratory syndrome virus, Virus Res. 154 (1) (2010) 18–30.
[28] D. Wang, J. Fan, L. Fang, R. Luo, H. Ouyang, C. Ouyang, et al., The nonstructural protein 11 of porcine reproductive and respiratory syndrome virus inhibits NF-kappaB signaling by means of its deubiquitinating activity, Mol. Immunol. 68 (2) (2015) 357–366.
[29] H. Zhang, Y. Chen, M. Liang, L. Xu, S. Qi, H. Chen, X. Chen, Solid-phase synthesis of highly fluorescent nitrogen-doped carbon dots for sensitive and selective probing ferric ions in living cells, Anal. Chem. 86 (19) (2014) 9846–9852.
[30] B. Li, S. Xiao, Y. Wang, S. Xu, Y. Jiang, H. Chen, et al., Immunogenicity of the highly pathogenic porcine reproductive and respiratory syndrome virus GP5 protein encoded by a synthetic ORF5 gene, Vaccine 27 (13) (2009) 1957–1963.
[31] S. Xiao, H. Chen, L. Fang, C. Liu, H. Zhang, Y. Jiang, et al., Comparison of immune responses and protective efficacy of suicidal DNA vaccine and conventional DNA vaccine encoding glycoprotein C of pseudorabies virus in mice, Vaccine 22 (3–4) (2004) 345–351.
[32] Q.L. Zhao, Z.L. Zhang, B.H. Huang, J. Peng, M. Zhang, D.W. Pang, Facile preparation of low cytotoxicity fluorescent carbon nanocrystals by electrooxidation of graphite, Chem. Commun. (41) (2008) 5116–5118.
[33] E. Duan, D. Wang, R. Luo, J. Luo, L. Gao, H. Chen, et al., Porcine reproductive and respiratory syndrome virus infection triggers HMGB1 release to promote inflammatory cytokine production, Virology 468–470 (2014) 1–9.
[34] R. Luo, L. Fang, H. Jin, Y. Jiang, D. Wang, H. Chen, et al., Antiviral activity of type I and type III interferons against porcine reproductive and respiratory syndrome virus (PRRSV), Antivir. Res. 91 (2) (2011) 99–101.
[35] L.J. Reed, H. Muench, A simple method of estimating fifty per cent endpoints, Am. J. Epidemiol. 27 (3) (1938) 493–497.
[36] K. An, L. Fang, R. Luo, D. Wang, L. Xie, J. Yang, et al., Quantitative proteomic analysis reveals that transmissible gastroenteritis virus activates the JAK-STAT1 signaling pathway, J. Proteome Res. 13 (12) (2014) 5376–5390.
[37] R. Zhang, L. Fang, D. Wang, K. Cai, H. Zhang, L. Xie, et al., Porcine bocavirus NP1 negatively regulates interferon signaling pathway by targeting the DNA-binding domain of IRF9, Virology 485 (2015) 414–421.
[38] X. Wang, K. Qu, B. Xu, J. Ren, X. Qu, Microwave assisted one-step green synthesis of cell-permeable multicolor photoluminescent carbon dots without surface passivation reagents, J. Mater. Chem. 21 (8) (2011) 2445–2450.
[39] L. Liu, L. Chen, J. Liang, L. Liu, H. Han, A novel ratiometric probe based on nitrogen-doped carbon dots and rhodamine B isothiocyanate for detection of Fe^{3+} in aqueous solution, J. Anal. Methods Chem. (2016) 4939582.
[40] Z.C. Yang, M. Wang, A.M. Yong, S.Y. Wong, X.H. Zhang, H. Tan, A.Y. Chang, X. Li, J. Wang, Intrinsically fluorescent carbon dots with tunable emission derived from hydrothermal treatment of glucose in the presence of monopotassium phosphate, Chem. Commun. 47 (42) (2011) 11615–11617.
[41] S. Chandra, P. Das, S. Bag, D. Laha, P. Pramanik, Synthesis, functionalization and bioimaging applications of highly fluorescent carbon nanoparticles, Nanoscale 3 (4) (2011) 1533–1540.
[42] H. Li, H. Ming, Y. Liu, H. Yu, X. He, H. Huang, K. Pan, Z. Kang, S.T. Lee, Fluorescent carbon nanoparticles: electrochemical synthesis and their pH sensitive photoluminescence properties, New J. Chem. 35 (11) (2011) 2666–2670.
[43] S.T. Yang, X. Wang, H. Wang, F. Lu, P.G. Luo, L. Cao, et al., Carbon dots as nontoxic and high-performance fluorescence imaging agents, J. Phys. Chem. C 113 (42) (2009) 18110–18114.
[44] S. Ray, A. Saha, N.R. Jana, R. Sarkar, Fluorescent carbon nanoparticles: synthesis, characterization, and bioimaging application, J. Phys. Chem. C 113 (43) (2009) 18546–18551.
[45] J. Ficinska, G. Van Minnebruggen, H.J. Nauwynck, K. Bienkowska-Szewczyk, H.W. Favoreel, Pseudorabies virus glycoprotein gD contains a functional endocytosis motif that acts in concert with an endocytosis motif in gB to drive internalization of antibody-antigen complexes from the surface of infected monocytes, J. Virol. 79 (11) (2005) 7248–7254.
[46] R. Naldinho-Souto, H. Browne, T. Minson, Herpes simplex virus tegument protein VP16 is a component of primary enveloped virions, J. Virol. 80 (5) (2006) 2582–2584.
[47] S. Wootton, G. Koljesar, L. Yang, K.J. Yoon, D. Yoo, Antigenic importance of the carboxy-terminal beta-strand of the porcine reproductive and respiratory syndrome virus nucleocapsid protein, Clin. Vaccine Immunol. 8 (3) (2001) 598–603.
[48] S.K. Wootton, D. Yoo, Homo-oligomerization of the porcine reproductive and respiratory syndrome virus nucleocapsid protein and the role of disulfide linkages, J. Virol. 77 (8) (2003) 4546–4557.
[49] C.R. Gomez, E.D. Boehmer, E.J. Kovacs, The aging innate immune system, Curr. Opin. Immunol. 17 (5) (2005) 457–462.
[50] G.C. Sen, Viruses and interferons, Ann. Rev. Microbiol. 55 (1) (2001) 255–281.
[51] T.S. Carlos, D. Young, S. Stertz, G. Kochs, R.E. Randall, Interferon-induced inhibition of parainfluenza virus type 5; the roles of MxA, PKR and oligo A synthetase/RNase L, Virology 363 (1) (2007) 166–173.
[52] E.C. Borden, G.C. Sen, G. Uze, R.H. Silverman, R.M. Ransohoff, G.R. Foster, et al., Interferons at age 50: past, current and future impact on biomedicine, Nat. Rev. Drug Discov. 6 (12) (2007) 975–990.
[53] X.X. Yang, C.M. Li, C.Z. Huang, Curcumin modified silver nanoparticles for highly efficient inhibition of respiratory syncytial virus infection, Nanoscale 8 (5) (2016) 3040–3048.
[54] X. Hang, H. Peng, H. Song, Z. Qi, X. Miao, W. Xu, Antiviral activity of cuprous oxide nanoparticles against hepatitis C virus in vitro, J. Virol. Methods 222 (2015) 150–157.
[55] L. Osminkina, V.Y. Timoshenko, I. Shilovsky, G. Kornilaeva, S. Shevchenko, M. Gongalsky, et al., Porous silicon nanoparticles as scavengers of hazardous viruses, J. Nanoparticle Res. 16 (6) (2014) 1–10.
[56] A. Barras, Q. Pagneux, F. Sane, Q. Wang, R. Boukherroub, D. Hober, et al., High efficiency of functional carbon nanodots as entry inhibitors for herpes simplex virus type 1, ACS Appl. Mater. Interfaces 8 (14) (2016) 9004–9013.
[57] T. Du, K. Cai, H. Han, L. Fang, J. Liang, S. Xiao, Probing the interactions of CdTe quantum dots with pseudorabies virus, Sci. Rep. 5 (2015) 16403.
[58] H. Wu, C. Mi, H. Huang, B. Han, J. Li, S. Xu, Solvothermal synthesis of green-fluorescent carbon nanoparticles and their application, J. Lumin. 132 (6) (2012) 1603–1607.
[59] S. Chandra, P. Das, S. Bag, D. Laha, P. Pramanik, Synthesis, functionalization and bioimaging applications of highly fluorescent carbon nanoparticles, Nanoscale 3 (4) (2011) 1533–1540.
[60] J. Zhou, Z. Sheng, H. Han, M. Zou, C. Li, Facile synthesis of fluorescent carbon dots using watermelon peel as a carbon source, Mater. Lett. 66 (1) (2012) 222–224.
[61] S. Sahu, B. Behera, T.K. Maiti, S. Mohapatra, Simple one-step synthesis of highly luminescent carbon dots from orange juice: application as excellent bio-imaging agents, Chem. Commun. 48 (70) (2012) 8835–8837.
[62] J. Wang, C.F. Wang, S. Chen, Amphiphilic egg-derived carbon dots: rapid plasma fabrication, pyrolysis process, and multicolor printing patterns, Angew. Chem. Int. Ed. 124 (37) (2012) 9431–9435.
[63] P. Pierrat, R. Wang, D. Kereselidze, M. Lux, P. Didier, A. Kichler, et al., Efficient in vitro and in vivo pulmonary delivery of nucleic acid by carbon dot-based nanocarriers, Biomaterials 51 (2015) 290–302.
[64] M.M. Titirici, R.J. White, N. Brun, V.L. Budarin, D.S. Su, F. del Monte, et al., Sustainable carbon materials, Chem. Soc. Rev. 44 (1) (2015) 250–290.
[65] H. Tao, K. Yang, Z. Ma, J. Wan, Y. Zhang, Z. Kang, et al., In vivo NIR fluorescence imaging, biodistribution, and toxicology of photoluminescent carbon dots produced from carbon nanotubes and graphite, Small 8 (2) (2012) 281–290.
[66] Z.A. Qiao, Y. Wang, Y. Gao, H. Li, T. Dai, Y. Liu, et al., Commercially activated carbon as the source for producing multicolor photoluminescent carbon dots by chemical oxidation, Chem. Commun. 46 (46) (2010) 8812–8814.
[67] S.N. Baker, G.A. Baker, Luminescent carbon nanodots: emergent nanolights, Angew. Chem. Int. Ed. 49 (38) (2010) 6726–6744.
[68] H. Ding, S.B. Yu, J.S. Wei, H.M. Xiong, Full-color light-emitting carbon dots with a surface-state-controlled luminescence mechanism, ACS Nano 10 (1) (2016) 484–491.